Journal of Rock Mechanics and Geotechnical Engineering xxx (xxxx) xxx

Contents lists available at ScienceDirect

Journal of Rock Mechanics and Geotechnical Engineering

journal homepage: www.jrmge.cn

Full Length Article

Shear behavior and off-fault damage of saw-cut smooth and tension-induced rough joints in granite

Fanzhen Meng [a], Feili Wang [a], Louis Ngai Yuen Wong [b,*], Jie Song [a], Muzi Li [a], Chuanqing Zhang [c], Liming Zhang [a,d]

[a] College of Science, Qingdao University of Technology, Qingdao, 266033, China
[b] Department of Earth Sciences, The University of Hong Kong, Pokfulam, Hong Kong, China
[c] State Key Laboratory of Geomechanics and Geotechnical Engineering, Institute of Rock and Soil Mechanics, Chinese Academy of Sciences, Wuhan, 430071, China
[d] Cooperative Innovation Center of Engineering Construction and Safety Shandong Peninsula Blue Economic Zone, Qingdao, 266033, China

ARTICLE INFO

Article history:
Received 15 February 2023
Received in revised form
25 April 2023
Accepted 9 July 2023
Available online xxx

Keywords:
Planar joint
Rough joint
Shear behavior
Off-fault damage
Micro-cracks

ABSTRACT

The damage of rock joints or fractures upon shear includes the surface damage occurring at the contact asperities and the damage beneath the shear surface within the host rock. The latter is commonly known as off-fault damage and has been much less investigated than the surface damage. The main contribution of this study is to compare the results of direct shear tests conducted on saw-cut planar joints and tension-induced rough granite joints under normal stresses ranging from 1 MPa to 50 MPa. The shear-induced off-fault damages are quantified and compared with the optical microscope observation. Our results clearly show that the planar joints slip stably under all the normal stresses except under 50 MPa, where some local fractures and regular stick-slip occur towards the end of the test. Both post-peak stress drop and stick-slip occur for all the rough joints. The residual shear strength envelopes for the rough joints and the peak shear strength envelope for the planar joints almost overlap. The root mean square (RMS) of asperity height for the rough joints decreases while it increases for the planar joint after shear, and a larger normal stress usually leads to a more significant decrease or increase in RMS. Besides, the extent of off-fault damage (or damage zone) increases with normal stress for both planar and rough joints, and it is restricted to a very thin layer with limited micro-cracks beneath the planar joint surface. In comparison, the thickness of the damage zone for the rough joints is about an order of magnitude larger than that of the planar joints, and the coalesced micro-cracks are generally inclined to the shear direction with acute angles. The findings obtained in this study contributes to a better understanding on the frictional behavior and damage characteristics of rock joints or fractures with different roughness.

1. Introduction

Fractured geological formations are ubiquitous in the rock mass. The presence of discontinuities in rock mass at different scales (fractures, bedding planes, joints and faults) not only controls the stability of rock tunnels and slopes (Barton and Choubey, 1977; Bandis et al., 1983; Hencher et al., 2011; Sainoki and Mitri, 2014; Meng et al., 2019; Zhang et al., 2022; Yang et al., 2022) but also provides pathways for the transport and flow of fluid and gas, thus having a great impact on the heat transfer and gas permeability (Barton and Quadros, 1997; Lee and Cho, 2002; Zhou et al., 2015; Vogler et al., 2016; Guo et al., 2016; Dang et al., 2019; Wang et al., 2022; Ji et al., 2022a, 2022b). The roughness of rock discontinuities is one of the most important factors that affect the shear behavior (e.g., shear strength, deformation, dynamic slip) and transport properties of jointed rock mass (Barton and Quadros, 1997; Barton and Choubey, 1977; Jiang et al., 2006; Zhao et al., 2014; Zielke et al., 2017; Yamashita et al., 2018; Dang et al., 2020, 2021; Wang et al., 2021, 2023; Xiu et al., 2023). Therefore, studying

* Corresponding author.
E-mail address: lnywong@hku.hk (L.N.Y. Wong).
Peer review under responsibility of Institute of Rock and Soil Mechanics, Chinese Academy of Sciences.

https://doi.org/10.1016/j.jrmge.2023.07.008

the degradation characteristics of the contacting asperities and the damage of the fault wall is of vital importance to advance our understanding of frictional slip process of rock joints under different mechanical, thermal and hydrological conditions.

The damage of rock joint or fault when subject to shear can be classified into two categories, namely superficial asperity damage on the surface and off-fault damage in the wall rock based on the location and distribution of the damage. Firstly, localized asperities degradation may occur on the raised asperities on the irregular and rough joint surface, the degree of which is dependent on the stress level and distribution pattern of the asperities. The results obtained from a number of acoustic and optical methods such as photo image analysis (Hong et al., 2016), three-dimensional surface laser scanning (Indraratna et al., 2014; Zhao et al., 2018) and acoustic emission monitoring (Wang et al., 2021, Meng et al., 2016, 2018, 2020a; Moradian et al., 2010, 2012) have shed light on the asperity damage characteristics and failure mechanism of asperities. These studies have shown that the amount of asperity degradation and gouge accumulation is positively related to the normal stress (Huang et al., 1993; Indraratna et al., 2014a, b; Hong et al., 2016; Meng et al., 2018). Moreover, only a small amount of asperity damage occurs prior to the peak shear stress, and most of the damage occurs in the post-peak stage (Grasselli et al., 2002; Moradian et al., 2012; Li et al., 2019; Meng et al., 2018).

The above studies mainly focus on the asperity damage on the joint surface. A damage zone, which consists of a large number of slip-induced micro-cracks may form beneath the shear interface in addition to the shear localization, especially when the normal stress is sufficiently high (Goebel et al., 2014a, 2014b; Passelègue et al., 2016a,b; Zhao et al., 2018). The damage zone can act as conduits of fluid flow or a barrier to flow depending on the internal heterogeneous texture and clay content (Rohmer et al., 2015). The mechanism, evolution, thickness and structural fabrics of fault damage zone have been well investigated in the realm of structural geology and earthquake dynamics by field studies at large scale (Ben-Zion and Sammis, 2003; Billi et al., 2003; Mitchell and Faulkner, 2009; Thomas et al., 2017). However, very limited laboratory studies have been conducted to illuminate the development of off-fault damage for rough joints/faults upon shear (Goebel et al., 2014a, 2014b; Passelègue et al., 2016a,b; Zhao et al., 2018), and little is known about the impact of factors such as stress level, roughness and rock texture on the initiation and extent of the off-fault damage. As the fault damage significantly influences the stability of the deep rock mass and the hydraulic transmissivity of the reservoir rocks and faults, further research on the evolution and influence factors of off-fault damage is highly warranted to cope with the increasing demands for subsurface deep natural resources exploitation (mining, natural gas, geothermal) and underground projects (tunnels, nuclear waste repository, CO_2 sequestration facilities).

Natural joints are usually rough, which can be described by self-similar and self-affine fractal models (Power and Tullis, 1991; Zhang et al., 2021). On the other hand, saw-cut surfaces, which are macroscopically planar, have been favorably used in rock mechanics and geophysics research communities in: (1) Determination of the basic friction angle of rock joint (Patton 1966; Hencher 2012; Mehrishal et al., 2016; Alejano et al., 2017, 2018; Li et al., 2019) in the shear strength model of JRC-JCS proposed by Barton (1973), the peak friction angle consists of dilation angle and basic friction angle, and the latter is essentially a measure of the adhesion of the flat surface and is dependent on the mineralogy (Li et al., 2019); and (2) Physical modeling of fault slip and earthquake nucleation process. Cubic or cylindrical rock blocks are first cut and the surfaces are then polished or roughened by silicon-carbide abrasives or sand paper with different grain sizes (Goebel et al., 2014a; Passelègue et al., 2016a,b; Lockner et al., 2017; Yamashita et al., 2018; Ji et al., 2020a; Ji and Wu, 2020b). These rock blocks are sheared under high pressure as simplified faults to reproduce a range of behavior. In the aforementioned first area of study, the damage of the joint is hardly of prevalent concern because of the typically low applied normal stress. In the above second area of study, a number of mechanisms, such as asperity melting, lubrication, flash heating, etc, have been generalized by observing and analyzing surface wear characteristics to account for the dynamic weakening of a fault under high normal stress or high slip velocity (Passelègue et al., 2016a,b; Chen et al., 2017; Lockner et al., 2017; Rowe et al., 2019; Dang et al., 2022). However, the off-fault damage of the simulated faults with saw-cut planar surface has rarely been investigated, and the correlation between the frictional behavior and the damage characteristics remains elusive. Moreover, the similarities and differences of the off-fault damage between the ubiquitous rough joints in nature and the extensively used saw-cut planar joints in laboratory also warrants further study.

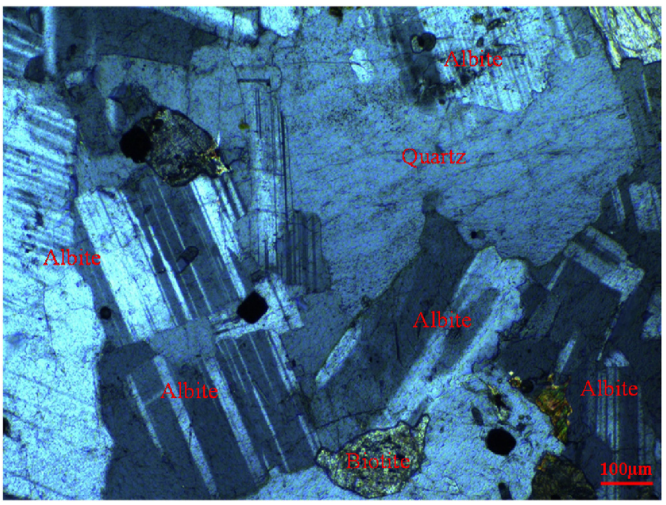

Fig. 1. Micro-structure of the used granite.

A number of studies have investigated the influence of surface roughness on the stick-slip failure (i.e. periodical shear stress build-up and sudden release) of fault, among which the saw-cut and polished surfaces with micron level roughness are popularly used (Okubo and Dieterich, 1984; Dieterich, 1978; Ohnaka and Shen, 1999; Zhou et al., 2020; Morad et al., 2020). Most of the studies have found that the greater the roughness, the smaller the stress drop during stick-slip. As the natural rock joint and fault are rough at different scales (at wavelengths from microns to tens of kilometers), and the roughness, such as the asperity, waviness and kinking, causes local variations in the stress and displacement fields near the fault, thus affecting the rupture growth and energy release. However, the difference between the shear behavior (such as slip mode, friction strength, roughness evolution, wear and damage characteristics) of the widely used saw-cut surfaces and the natural rough surfaces has scarcely been investigated, which warrants a more elaborate study.

In view of the above research limitations and knowledge gap, we choose the planar granite surfaces with almost no perceptible roughness, and tension-induced rough granite surfaces with irregular morphology (rather than using polished surfaces with micron-sized roughness) to conduct the direct shear test under normal stress ranging from 1 MPa to 50 MPa. The frictional behavior of the two different types of rock surface is firstly investigated, and influence of surface condition on the shear behavior (e.g., shear strength, stick-slip, etc) is particularly discussed. The

Please cite this article as: Meng F et al., Shear behavior and off-fault damage of saw-cut smooth and tension-induced rough joints in granite, Journal of Rock Mechanics and Geotechnical Engineering, https://doi.org/10.1016/j.jrmge.2023.07.008

obtained results are also compared with previous results using rock surface with micron scale roughness. Furthermore, the shear-induced off-fault fracturing damage inside the wall rock is examined on the post-experimental thin-sections using an optical microscope, and the effects of normal stress and surface condition on the thickness of the damage zone are studied. The correlation between the macro-frictional behavior and the micro-damage characteristics are further explored.

2. Material and methods

X-ray diffraction analysis shows that the test granite is composed of quartz (20.4%), albite (44.1%), biotite (24.1%), hornblende (6.9%), and maghemite (4.5%), with an average grain size of about 0.75 mm (Fig. 1). The micro-structure of the granite without shear shows that individual grains are distinguishable and in intimate contact. Inherent micro-cracks are also rare within the mineral.

Specimens of two dimensions (length × width × height: 100 mm × 100 mm × 100 mm, and 100 mm × 100 mm × 55 mm) are cut from a large rock block, and the six surfaces of the cubic specimens are all ground in general accordance with the method suggested by the International Society for Rock Mechanics and Rock Engineering (ISRM) (Muralha et al., 2014). Similar to the Brazilian Splitting test procedures, the cubic specimens with dimensions of 100 mm × 100 mm × 100 mm are then split by applying a pair of linear loads on the two opposite and parallel surfaces to create a pair of matching tension-induced rough fractures (Fig. 2) in our study (Meng et al., 2016). As there is insignificant damage (limited chippings, gouges and microcracks) on the tension-induced fractures (Meng et al., 2022a), those damage (asperity wear and off-fault fracturing) after shear tests can be regarded to be attributed to the shear process in our study. Therefore the rationale of using tension-induced fracture rather than shear induced fracture in our study is to avoid the confusion arising from the pre-existing damage (from the specimen preparation process) and the shear induced damage. A saw-cut planar joint is formed by stacking two blocks with the same dimensions (i.e. 100 mm × 100 mm × 55 mm) (Fig. 2). The smoothness of the shear surface for the planar joint is the same as other surfaces of the cubic blocks.

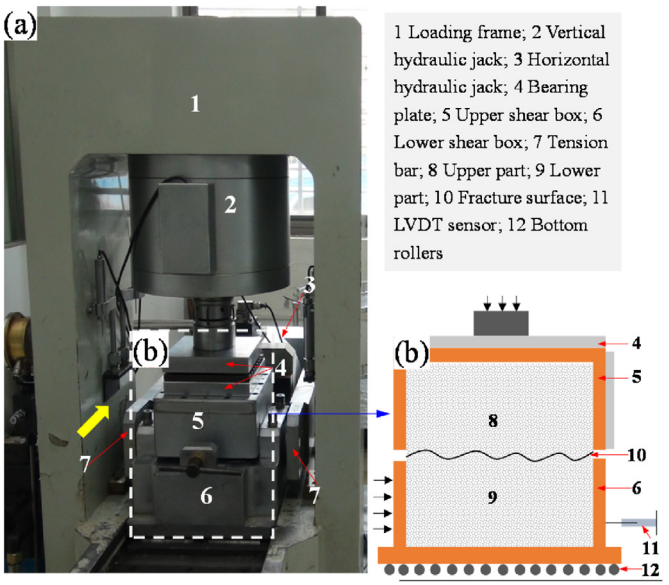

Fig. 3. RMT150C rock testing system. The right image shows the schematic diagram of the shear boxes enclosed by the rectangle in the left image.

Before the direct shear test, the roughness of the joint surfaces is quantified by the RMS of the asperity height (Eq. (1)). For the planar joint, the surface roughness is measured by the Taylor Hobson-PGI 800 with resolution of 0.8 nm. The RMS along the shear direction does not differ much when 5 mm- and 10 mm-wavelengths are separately measured (Fig. 2f), indicating that the roughness of the planar surface is scale-invariant (Power and Tullis, 1991). Due to the similarity of the RMS for the planar surface, only two profiles with length of 5 mm and 10 mm are scanned, and the average RMS is taken as the roughness of the plane:

$$\mathrm{RMS}_x = \left[\frac{1}{L}\int_0^L Y^2(x)\mathrm{d}x\right]^{0.5} \quad (1)$$

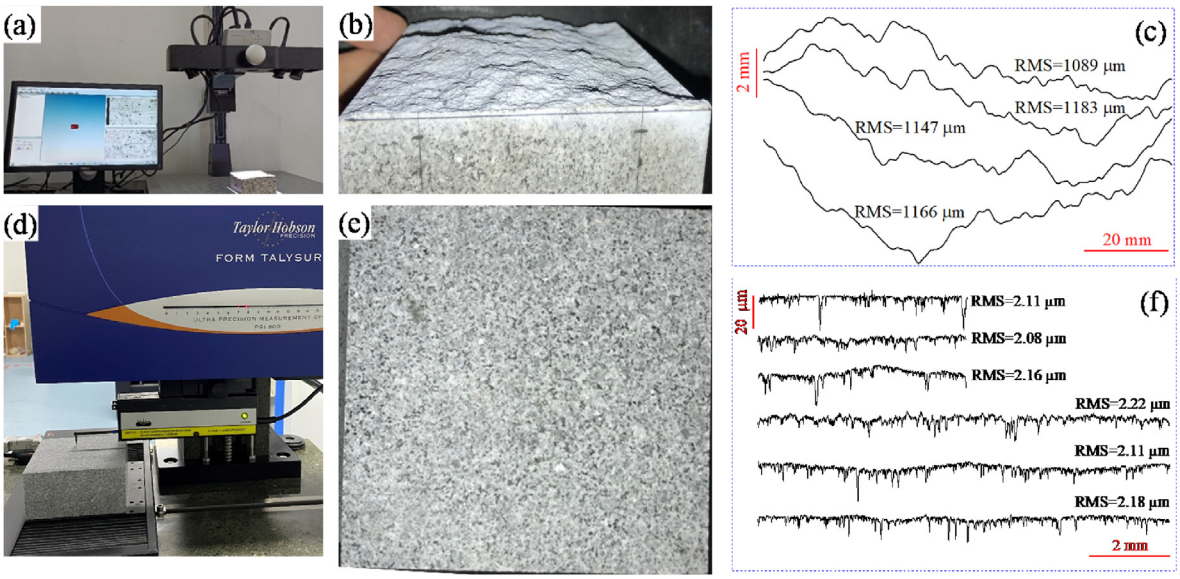

Fig. 2. (a) Holon^{3D} optical scanning system, (b) Tension-induced rough joint surface, (c) Four profiles of (b) and the corresponding root mean square (RMS), (d) Taylor Hobson-PGI 800 scanner, (e) Saw-cut planar joint surface, and (f) Several representative profiles (with wavelength of 5 mm and 10 mm) and the corresponding RMS of the planar joint surface.

Please cite this article as: Meng F et al., Shear behavior and off-fault damage of saw-cut smooth and tension-induced rough joints in granite, Journal of Rock Mechanics and Geotechnical Engineering, https://doi.org/10.1016/j.jrmge.2023.07.008

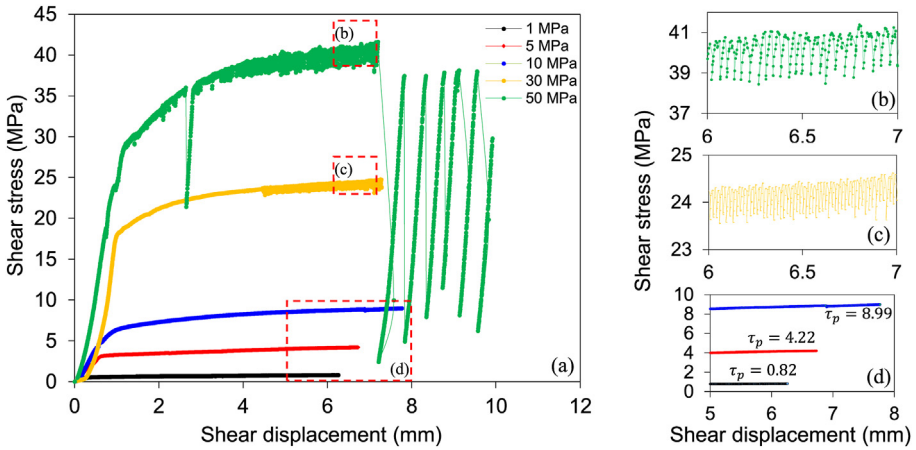

Fig. 4. (a) Shear stress-shear displacement curves of saw-cut planar joints under different normal stresses, (b), (c) and (d) are the zoom-in view of stress curves b, c and d as enclosed by the rectangles in (a). The peak shear strength is marked on the stress curves in (d).

where L is the profile length, Y is the amplitude of a given point, and x is the distance along the profile in a given direction. The RMS value for the planar joints used in this study is around 2 μm.

The surfaces of the rough joints are scanned by the Holon^{3D} optical scanning system, and the data cloud is used to digitize and reconstruct the fracture surfaces. Compared with the planar joint surface, the tension-induced fracture surface is usually characterized by irregular morphology, and the roughness is also dependent on the measuring scale (Power and Tullis, 1991). Therefore, for the rough surface, the RMS of ten parallel 100 mm long profile lines equally spaced at 10 mm along the shear direction is calculated based on Eq. (1), and the average RMS is used to characterize the overall roughness of the surface. The RMS values for the rough joints range from 1200 μm to 2250 μm.

Direct shear tests are conducted on the RMT150 system (Fig. 3). Shear load is remotely applied by the horizontal hydraulic jack with the maximum loading capacity of 500 kN, and the sampling interval of data acquisition for the shear load is 0.8 s. The shear displacement is monitored by a linear variable differential transformer (LVDT) sensor attached on the lower shear box (Fig. 3). During the shear tests, the lower shear box is pulled by the two tension bars on its two sides, while the upper shear box remains stationary in the horizontal direction. For the saw-cut planar joints, a normal stress of 1 MPa, 5 MPa, 10 MPa, 30 MPa or 50 MPa is applied. As the shear strength of rough joints under 50 MPa normal stress is very likely to exceed the maximum shear load of the test system, the normal stress is therefore only set at 1 MPa, 5 MPa, 10 MPa, 20 MPa and 30 MPa respectively without 50 MPa. At the beginning of the test, the normal load is applied at 1 kN/s until reaching the target value. The shear load is then applied at 0.002 mm/s while keeping the normal load constant.

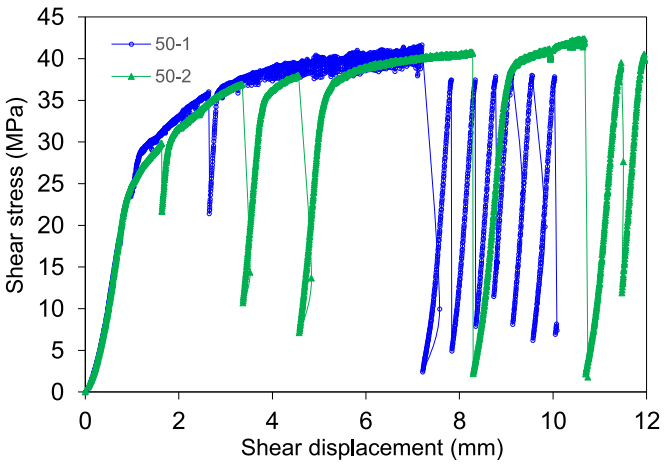

Fig. 5. Comparison of two shear stress-shear displacement curves under the normal stress of 50 MPa (50-1 and 50-2 indicate the first and second joints).

To study the microscopic damage characteristics of the fault after shear, thin-sections (about 30 mm long and 20 mm wide) perpendicular to the joint plane along the shear direction are prepared by cutting the lower part of the specimen. As the surface wear appears uniform for the saw-cut planar surface, the location of the thin-section is chosen approximately in the center of the specimen. However, shear localization usually occurs on the surface of the rough joints, and the damage on the surface is not evenly distributed. We therefore choose sites with remarkable wear, which are not necessarily located at the center, for preparing the thin-sections (refer to Section 3.3 for more details). One thin-section is prepared for each planar joint, and one or two thin-sections (the two thin-sections are located at different sites) are prepared for each rough joint.

3. Results and analysis

3.1. Shear behavior of joints

3.1.1. Saw-cut planar joints

The shape of the shear stress-shear displacement curves is similar when the planar joints are sheared under low normal stresses (1 MPa, 5 MPa and 10 MPa) (Fig. 4a). The shear stress has been corrected to cater for the decrease of the contact area between the upper and lower parts during shear. The shear stress first increases with the shear displacement, after which it becomes less dependent on the shear displacement (Fig. 4d). The shear stress curve under the normal stress of 30 MPa is similar to that of joints sheared under lower normal stresses (1 MPa, 5 MPa and 10 MPa) when the shear displacement is less than 4.4 mm, after which the shear stress shows some fluctuation. Fig. 4c is the zoom-in view of the stress curve under the normal stress of 30 MPa in Fig. 4a, which clearly shows the increase and decrease of intermittent stress, i.e. stick-slip. The overall shape of the stress curve is similar to others except the very large stress drops close to the end of the tests when the normal stress increases to 50 MPa (this joint will be named as 50-1 thereafter). Moreover, its stress oscillation is much more

Please cite this article as: Meng F et al., Shear behavior and off-fault damage of saw-cut smooth and tension-induced rough joints in granite, Journal of Rock Mechanics and Geotechnical Engineering, https://doi.org/10.1016/j.jrmge.2023.07.008

remarkable, and the stress drop value becomes larger and the interval of each stress drop becomes longer than that under 30 MPa normal stress (Fig. 4b).

As compared with other planar joints, a stress drop occurs when shear displacement reaches 2.8 mm for joint 50-1, then the shear stress quickly restores to a level comparable to that before the stress drop. We consider that this stress drop is associated with the local fracture and spalling of the specimen under high normal stress. The very intense stick-slip towards the end of the shear test does not occur in other planar joints.

To check the reproducibility of the test result under the normal stress of 50 MPa, another planar joint (named as joint 50-2 thereafter) is sheared under the same test condition. The overall trend of shear stress and the peak shear strength of these two planar joints are very similar (Fig. 5). The most remarkable difference between the two curves is that there are four stress drops preceding the last two regular stick-slip for joint 50-2, while there is only one stress drop for joint 50-1. After the stress drop, the shear stress gradually recovers to the stress level which is comparable to the shear stress without stress drops. The slope of the stress recovery period is similar to that of the initial loading stage. Similar to joint 50-1, towards the end of the test, stick-slip occurs. The causes that lead to the different behavior of the two joints sheared under 50 MPa normal stress will be discussed in detail in Section 4.

The post-shear surfaces of the saw-cut planar joints undergo different degrees of wear under different normal stresses (Fig. 6). Almost no macroscopical wear traces are found on the surface under the normal stress of 1 MPa (Fig. 6a), and not much difference exists between the post-shear and pre-shear surface. Under the normal stress of 5 MPa, the individual minerals on the post-shear surface become less identifiable as compared with that under the normal stress of 1 MPa. However, no remarkable wear traces are found (Fig. 6b). When the normal stress is greater than 5 MPa, a number of parallel wear traces along the shear direction are clearly observed (Fig. 6c–f). The color of the surface turns from pale white to dark grey, which is attributed to the more severe grinding and

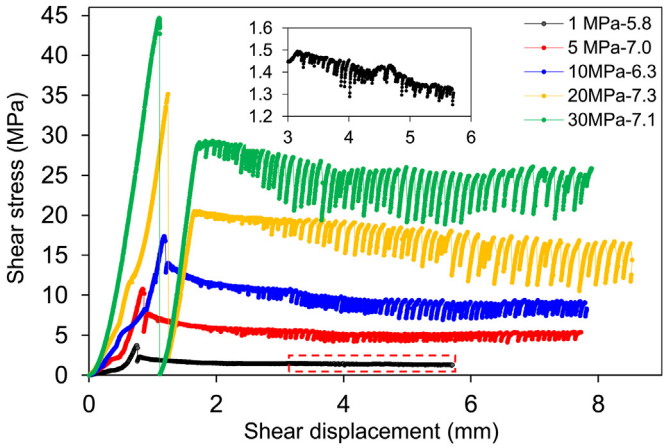

Fig. 7. Shear stress-shear displacement curves of the tension-induced rough joints under different normal stresses. The inset is the zoom-in view of the stress curve under the normal stress of 1 MPa enclosed by the rectangle. The short horizontal lines indicate the residual shear strengths.

damage of the biotite with increasing normal stress. Three white patches in Fig. 6f are related to three large fractures (Fig. 6g) that propagate into the host rock (will be further discussed in Section 4).

3.1.2. Tension-induced rough joints

The shear behavior of rough joints is strikingly different from that of the planar joints in the following aspects (Fig. 7): (1) The peak shear strength of rough joints is much greater than that of the planar joints under the same normal stress; (2) Each stress-displacement curve of the rough joint contains a prominent peak followed by an abrupt drop, after which the shear stress gradually recovers; and (3) In the frictional sliding stages, regular stick-slip occurs on all joints (under 1 MPa normal stress, the amplitude of the stick-slip is small, as shown in the inset of Fig. 7). These

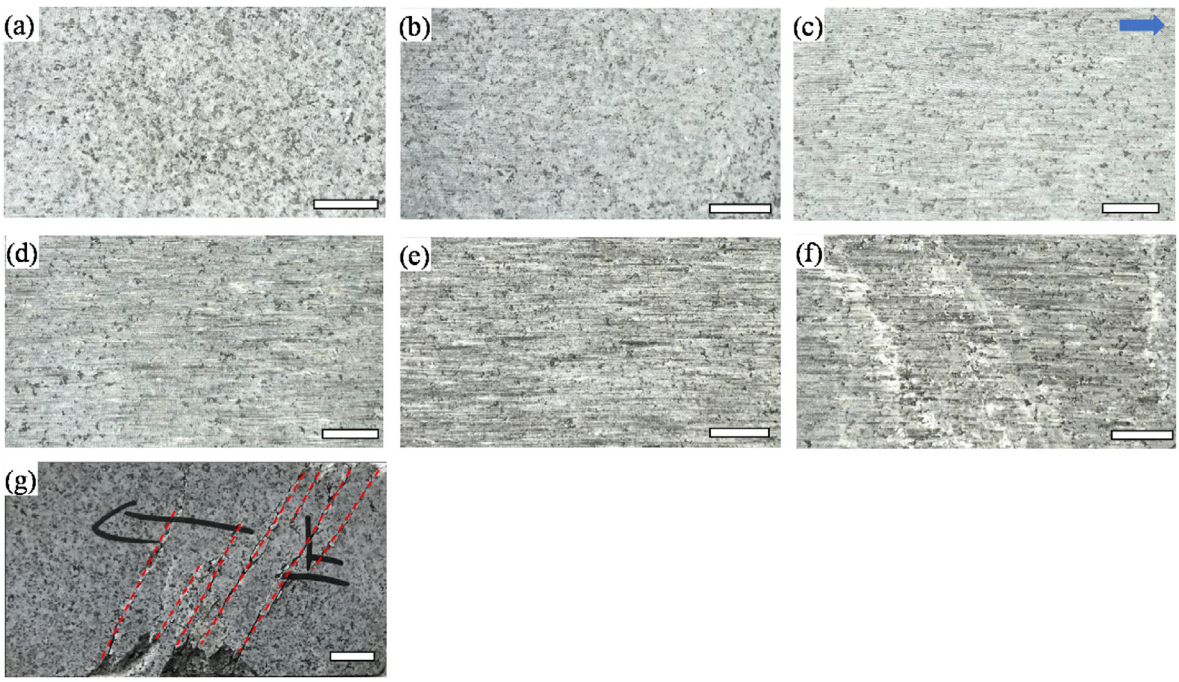

Fig. 6. Surface wear and wall rock damage characteristics of the saw-cut planar joints sheared under (a) 1 MPa, (b) 5 MPa, (c) 10 MPa, (d) 30 MPa, (e) 50 MPa (50-1), (f) 50 MPa (50-2), and (g) Wall rock damage of joint 50-2. The arrow at the top right indicates the shear direction, and length of the scale bar is 10 mm.

Please cite this article as: Meng F et al., Shear behavior and off-fault damage of saw-cut smooth and tension-induced rough joints in granite, Journal of Rock Mechanics and Geotechnical Engineering, https://doi.org/10.1016/j.jrmge.2023.07.008

characteristics are consistent with the findings on different granite types in our previous studies (Meng et al., 2016, 2018).

Fig. 8 shows the post-shear surfaces of the rough joints (lower block) sheared under normal stresses of 1 MPa, 10 MPa and 30. The number of damaged regions, which appear as white patches covered by powders, increases with increasing normal stress. A larger number of small damaged regions are observed under the normal stress of 1 MPa, indicating that the asperity tips on the irregular joint surface are crushed or sheared off upon shear. Under elevated normal stresses, the small regions coalesce into large patches, suggesting that the number and depth of the damaged asperities increase.

3.1.3. Strength envelope

Variation of the peak shear strength, residual shear strength of the rough joints, and peak shear strength of the planar joints with increasing normal stress are shown in Fig. 9. Since each peak of the stick-slip sliding does not vary much with increasing shear displacement for a rough joint, the peak of the stick-slip in the shear stress curves is taken as the residual shear strength (Fig. 7). The shear stress of the planar joint still shows a slightly increasing trend at the end of the test, which we consider is because the surface gradually becomes rougher with increasing shear displacement (Section 3.2 for more detail). Therefore, the shear stress close to the end of the shear test is taken as the peak shear strength for the planar joints (Fig. 4d).

The relation between the shear strength and the normal stress is well fit by the linear Mohr-Coulomb failure criterion. The difference between the peak and residual shear strength becomes larger with increasing normal stress. The peak friction angle is 55° as compared with the residual friction angle of 40°. The residual strength envelope of the rough joints and the shear strength envelope of the planar joints almost overlap, which indicates that the residual friction angle of rough joints provides a good approximation of the basic friction angle determined by direct shear tests on saw-cut planar joints.

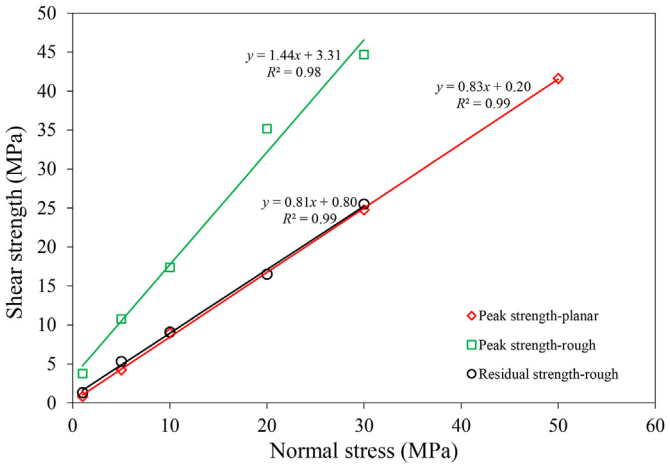

Fig. 9. Variation of peak shear strength and residual shear strength for rough joints, and peak shear strength for planar joints.

3.2. Changes in roughness after shear

To compare the surface roughness before and after shear, the gouge and debris on the post-shear rough surfaces are first cleaned by a very soft toothbrush, after which the surface is scanned again with the Holon^{3D} optical scanning system to obtain the RMS roughness along the shear direction. For the planar joints, only the post-shear surfaces under normal stresses of 1 MPa, 10 MPa and 30 MPa are scanned by the Taylor Hobson-PGI 800 to calculate the RMS (other specimens had been discarded after cutting for preparing thin-sections). In particular, RMS values along two directions, namely the direction parallel with ("P" in Fig. 10) and perpendicular to ("V" in Fig. 10) the shear direction are analyzed and compared.

As the rough joints are obtained by artificial splitting, the RMS before shear shows large diversity compared with the planar joints. The result in Fig. 10a shows that RMS of all the five rough joints decreases after shear, while it increases for the three planar joints regardless of the analysis direction. A larger normal stress generally leads to more degradation of the RMS for rough joints (Fig. 10b), indicating that the surface becomes much smoother. On the other hand, the surface of the planar joint becomes rougher under a higher normal stress. The increase in RMS is more prominent along the perpendicular direction than parallel direction, and the underlying mechanism will be further discussed in section 4.1.

3.3. Off-fault fracturing damage

A straight line (about 30 mm long) parallel with the shear direction is first drawn on the post-shear joint surface (Fig. 8, as indicated by the red lines). The specimen is then cut into two pieces along this line, and a thin-section (about 30 mm long and 20 mm wide) is made beneath this line. A preliminary comparison of the thin-section images of the post-shear planar and rough joints shows that the micro-cracks are much fewer in the planar joints than in the rough joints. Therefore, two different methods are

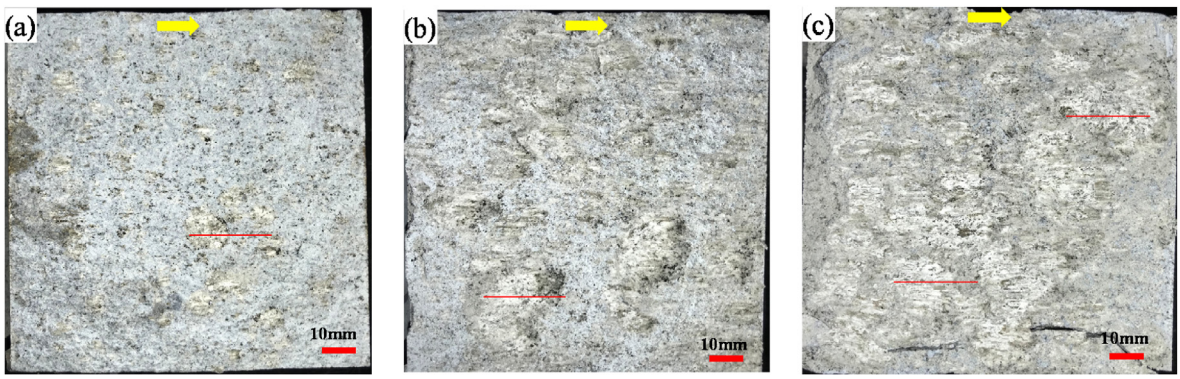

Fig. 8. Surface damage characteristics of the tension-induced rough joints under different normal stresses of (a) 1 MPa, (b) 10 MPa and (c) 30 MPa (the red lines indicate the location for making thin-sections, refer to section 5 for details).

Please cite this article as: Meng F et al., Shear behavior and off-fault damage of saw-cut smooth and tension-induced rough joints in granite, Journal of Rock Mechanics and Geotechnical Engineering, https://doi.org/10.1016/j.jrmge.2023.07.008

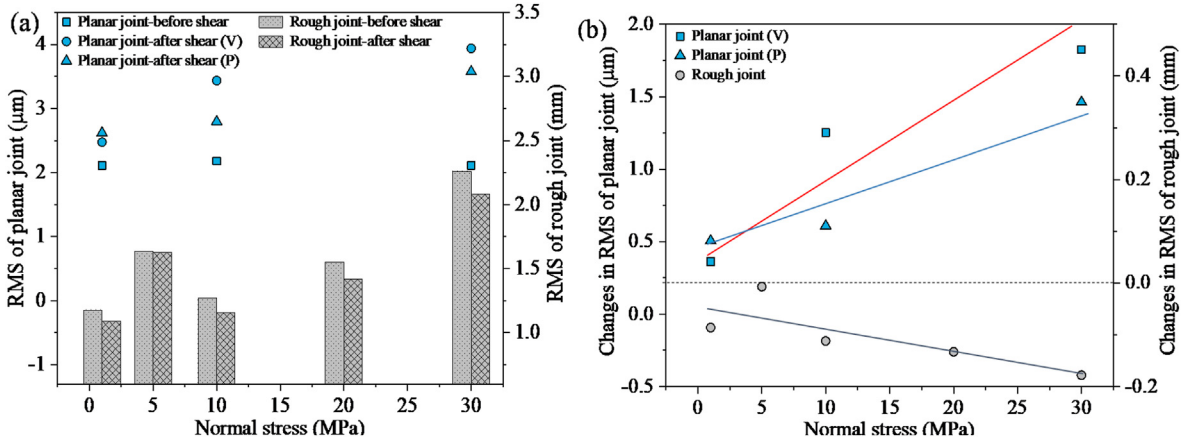

Fig. 10. (a) RMS roughness before and after shear, and (b) Changes in RMS roughness after shear for tension-induced rough joint surfaces and planar surfaces. "V" and "P" indicate vertical to and parallel with the shear direction respectively, and the three lines in (b) show the increasing or decreasing tendency.

separately used to examine and quantify the damage zone size of the two joint types.

For the planar joints, liquid epoxy resin is applied onto the post-shear surface after shear to cover the area which is marked by the red line to preserve the original state of the post-shear surface and protect it from damage during cutting (Fig. S1). The epoxy resin can permeate into the void and fractures (if any) beneath the planar surface, and the thickness of this area which is filled with epoxy resin is taken as the indicator to estimate the damage level of the planar surface.

To expose the underlying surface of the rough joint surfaces after shear, the debris and gouge generated from shear are cleaned before scanning. Therefore, the post-shear surfaces were not coated with the epoxy resin for the rough joints. We used a more accurate method to determine the damage zone width. First, the interested zone with an area of 5 mm × 12.8 mm is selected from the large panoramic thin-sections (35 mm × 19 mm), and a number of parallel vertical and horizontal lines with equal spacing of 0.2 mm were drawn on the thin-section images to form square grids (Fig. S2). Then, if there is one or more cracks in the square, this square will be counted as 1. In one row, the total number of squares that contain cracks can be obtained ($N_{crack} = 1 + 1{+}1 + 1 \ldots$), and the relative crack density (ρ_r) at this horizontal line is defined as the ratio of N_{crack} to the total number of squares N_{total}. Along the direction perpendicular to the shear surface, ρ_r at different locations (i.e. rows) can then be obtained. The width of the damage zone is determined as the distance from the shear interface to the location where ρ_r becomes not significantly influenced by the distance. As the size of the square is quite small (the line spacing is only 0.2 mm), this method can effectively evaluate the distribution of the microcracks in the wall rock of the joint.

3.3.1. Saw-cut planar joint

When the planar joint is respectively sheared under the normal stress of 1 MPa and 5 MPa, the micro-structure (Fig. 11a and b) shows little difference from that of the rock without shear. Microcracks are rarely observed within the region close to the shear surface. It is worth noting that the planar surface becomes microscopically rougher after shear, which is attributed to the wear damage during shear as well as the damage which incurs on the surface during rock cutting process.

The sub-horizontal pink line close to the top of each sub-figure (Fig. 12a and b) is drawn after the shear test to mark the cutting location (Fig. S1, the red line beneath the epoxy resin). The very smooth and planar appearance indicates that the epoxy resin is very effective to preserve and protect the post-shear surface during sample preparation. Fig. 12–14 show that the epoxy resin has permeated into the voids and apertures beneath the planar surface (the red dashed line traces the boundary between the surface epoxy resin and the minerals beneath in these figures). The circles in the regions are the bubbles sealed in the epoxy resin. The comparison of Figs. 11 and 12 shows that those parts above the boundary (i.e. red dashed line) probably will not be preserved and observed if the post-shear specimen is cut directly without the epoxy treatment.

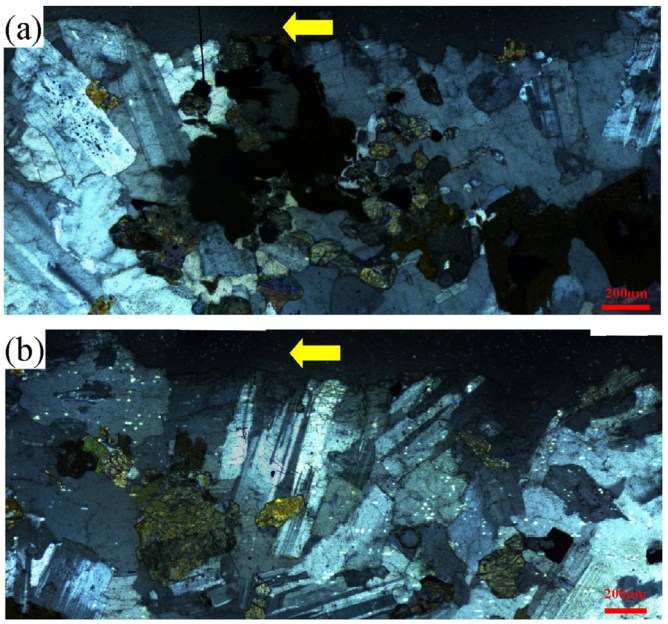

Fig. 11. Micro-structure within the fault wall of planar joints under normal stresses of (a) 1 MPa and (b) 5 MPa (the shear interface is on the top of the images, and the yellow arrow in Fig. 11–14 indicates the shear direction).

Under the normal stress of 10 MPa (Fig. 12), the thickness of the damage zone in the lower part of the joint is approximately in the range of 0–440 μm. The variation of the damage thickness indicates that the shear stress is heterogeneous even for the very planar joint surface. The minerals below the dashed lines are relatively intact with insignificant damage, which indicates that the influence of shear is predominantly restricted to a very thin top layer of the planar surface.

Please cite this article as: Meng F et al., Shear behavior and off-fault damage of saw-cut smooth and tension-induced rough joints in granite, Journal of Rock Mechanics and Geotechnical Engineering, https://doi.org/10.1016/j.jrmge.2023.07.008

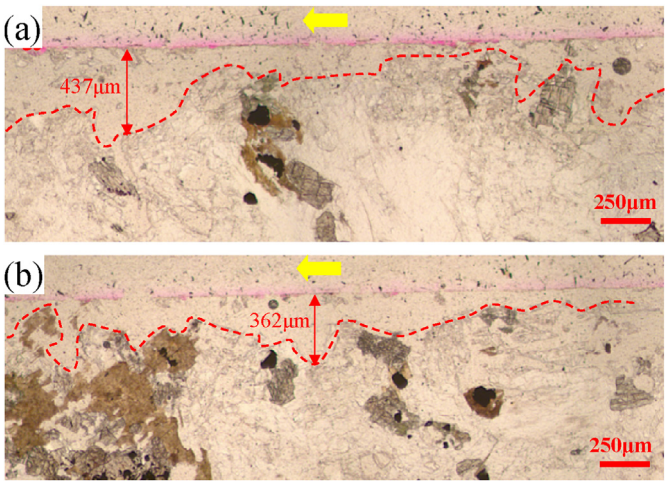

Fig. 12. Micro-structure within the fault wall of planar joint under 10 MPa normal stress, (a) and (b) are from different parts of the same thin-section containing the shear surface (the red dashed line indicates the boundary between the epoxy resin layer and the minerals, so as in the subsequent figures).

The micro-structures of the joint surface, which has been sheared under the normal stress of 30 MPa, observed under cross- and plane-polarized light are shown in Fig. 13a–d. Similar to those shown in Fig. 12, epoxy resin can be observed below the straight red line, the maximum depth of which is about 600 μm in the observation range (Fig. 13e). The generated gouges on the surface are not cleaned before applying the epoxy resin. Some rock debris above the epoxy resin therefore can be observed.

Under the normal stress of 50 MPa, the key characteristics of the micro-structure (Fig. 14) are similar to those shown in Figs. 12 and 13, and the maximum thickness of the permeant epoxy resin (i.e. the thickness of the damage zone) in the viewing zone is about 700 μm (Fig. 14b). Several small bubbles are observed on the right side of Fig. 14a and b, which are resulted from the infiltration and flow of the epoxy resin through connected cracks.

3.3.2. *Tension-induced rough joint*

Fig. 15–18 show post-shear micro-structure within the fault wall and the variation of ρ_r with increasing distance of rough joints under normal stresses of 1 MPa, 10 MPa, 20 MPa and 30 MPa, and ρ_r decreases with the distance away from the shear surface approximately following the power law. A small number of micro-cracks which are randomly distributed adjacent to the upper surface can be observed in the mineral grains when the rough joint is sheared under the normal stress of 1 MPa (Fig. 15a). These cracks are short and unordered, usually shorter than the dimensions of the mineral grains (Fig. 15b). The micro-cracks are predominately distributed within 0.6–1 mm away from the top surface (Fig. 15c).

More minerals are cracked after shear under the normal stress of 10 MPa (Fig. 16a), and a greater number of stress-induced micro-cracks develop in the minerals near the top surface than those under a lower normal stress. These cracks appear unordered at a cursory glance. However, the enlarged view in Fig. 16b shows that these coalesced cracks that traverse the mineral grains are generally inclined to the shear direction with acute angles. The variation of ρ_r with increasing distance indicates that thickness of the shear-induced off-fault damage zone increases to about 4.6 mm (Fig. 16c).

The maximum thickness of the damage zone in the viewing zone increases to about 5.2 mm under normal stress of 20 MPa (Fig. 17b). On the other hand, the minerals on the right side of Fig. 17a appear to be less influenced by shear, which is inferred from the small number of micro-cracks. The relative crack density ρ_r is smaller on the right side than that on the left side (Fig. 17b), and the determined damage zone width is also smaller (2 mm vs 5.2 mm). This indicates that the non-uniform stress distribution on the rough surface can lead to different degrees of damage at different regions.

Under the normal stress of 30 MPa, the micro-cracks are ubiquitous in the viewing area (Fig. 18a). However, these micro-cracks have not coalesced to form the macro-fractures in the cataclastic minerals, and there seems no preferential direction for their development for most of the micro-cracks. However, a careful examination in the regions near the shear surface indicates that these micro-cracks are generally inclined to the shear direction with acute angles (the red arrows in Fig. 18a and b), which is similar to those in Fig. 16. The maximum thickness of the damage zone reaches about 11.4 mm.

As we do not use epoxy resin to coat the post-shear surface, those small fractured mineral grains on the top layer of the surface probably have been removed from the host rock during rock cutting and hence not observed in the thin-section images. Besides, the tips of some asperities are sheared off during shear, and the generated gouges are then cleaned after shear before cutting. Therefore the true thickness of the damage zone would be slightly larger than the estimated size as discussed above.

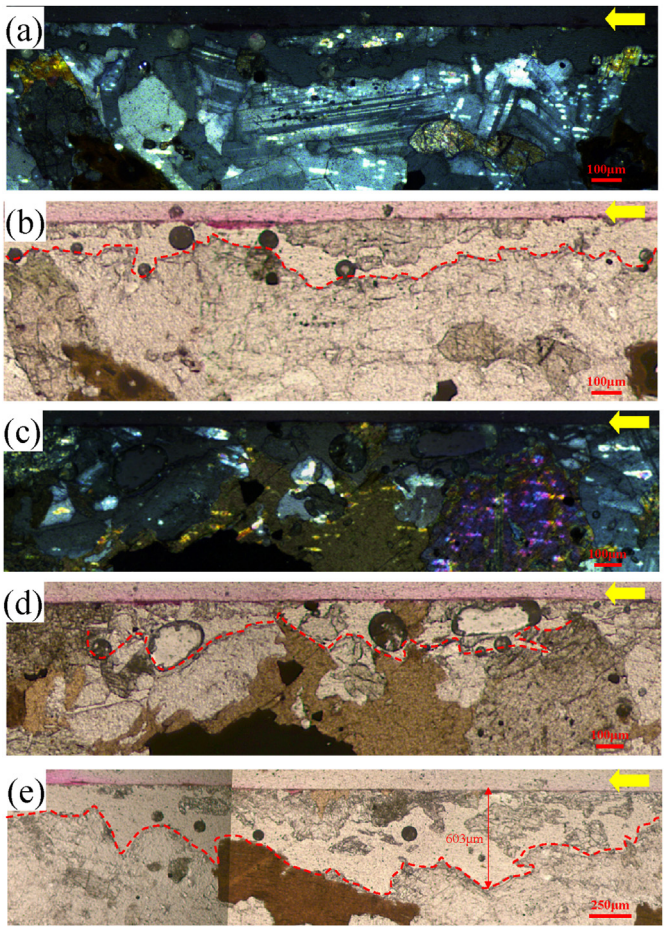

Fig. 13. Micro-structure within the fault wall of planar joint under the normal stress of 30 MPa. The dark circles above the dashed line are the bubbles sealed in the epoxy resin: (a), (c) and (e) are different parts of the same thin-section containing the shear surface, (b) and (d) are the plane-polarized thin-section images of (a) and (c).

Please cite this article as: Meng F et al., Shear behavior and off-fault damage of saw-cut smooth and tension-induced rough joints in granite, Journal of Rock Mechanics and Geotechnical Engineering, https://doi.org/10.1016/j.jrmge.2023.07.008

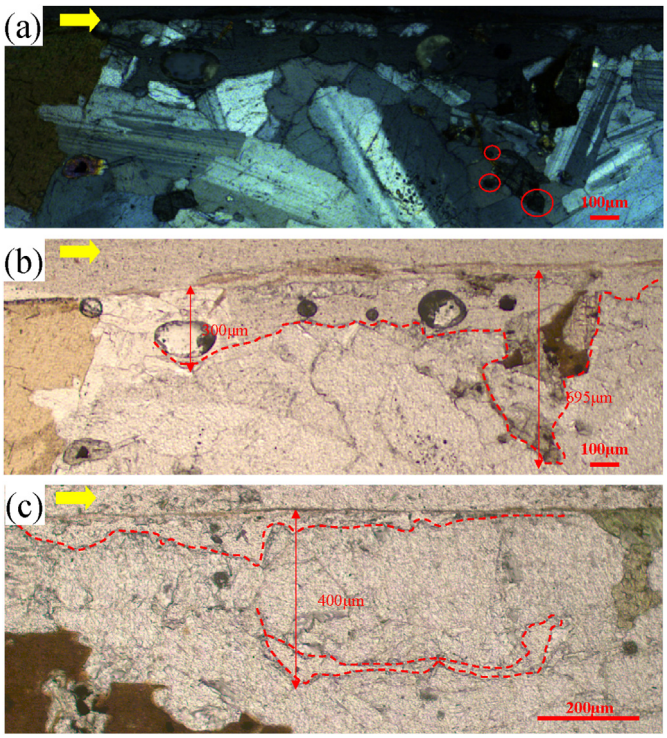

Fig. 14. Micro-structure within the fault wall of planar joint under the normal stress of 50 MPa (50-1): (a) and (c) are from different parts of the same thin-section containing the shear surface, and (b) is the plane-polarized thin-section image of (a).

4. Discussion and implication

4.1. Comparison of micro-damage for planar and rough joints

The above analyses indicate that the surface becomes rougher after shear for the initially smooth and planar joints, and the increase in roughness is more significant in the direction vertical to the shear direction than along the shear direction. Fig. 6 shows that parallel wear grooves occur on the surface after shear, and the micro-observation in Figs. 12–14 indicate that the generated grooves are filled with epoxy resin. The depth of the groove varies with different locations even for the same surface but is much greater than the original asperity height before shear (Fig. 2f), and it also generally increases with increasing normal stress. These phenomena can account for the increase in roughness after shear along the shear direction. Besides, there are usually rock ridges between two adjacent microgrooves, and the altitude of the ridges is larger than the base of grooves. The undulating topography leads to more significant increase in roughness along the vertical direction than the parallel direction.

The off-fault damage for the rough joints usually consists of two parts based on the location of the damage. The first part is similar to that of the planar joints, which occurs in the immediate vicinity of shear interface (for the planar joint, this damage is preserved beneath the epoxy resin coating, and can be observed by the optical microscope). As some of the asperity tips are cut off, and the generated gouges have been removed after test, this part of damage cannot be observed in the thin-section images. The shear-off of the rough asperity tips causes the decrease of roughness after shear (Fig. 10). The second part of damage occurs next to and below the first one. The damage described in Section 3.3.2 all belongs to this part. For the planar joints, there is almost no damage that pertains to the second part.

The estimated maximum thickness of the damage zone is usually less than 1 mm for the planar joints (e.g. it is 0.44 mm and 0.6 mm for the joints respectively sheared under normal stresses of 10 MPa and 30 MPa). In contrast, the thickness increases to 4.6 mm and 11.4 mm when the rough joints are sheared under normal stresses of 10 MPa and 30 MPa, respectively, which indicates that the thickness of the damage zone for the rough joints is about an order of magnitude greater than that of the saw-cut planar joints. The larger damage zone for the rough fractures is attributed to the much larger stress concentration on the large asperities during

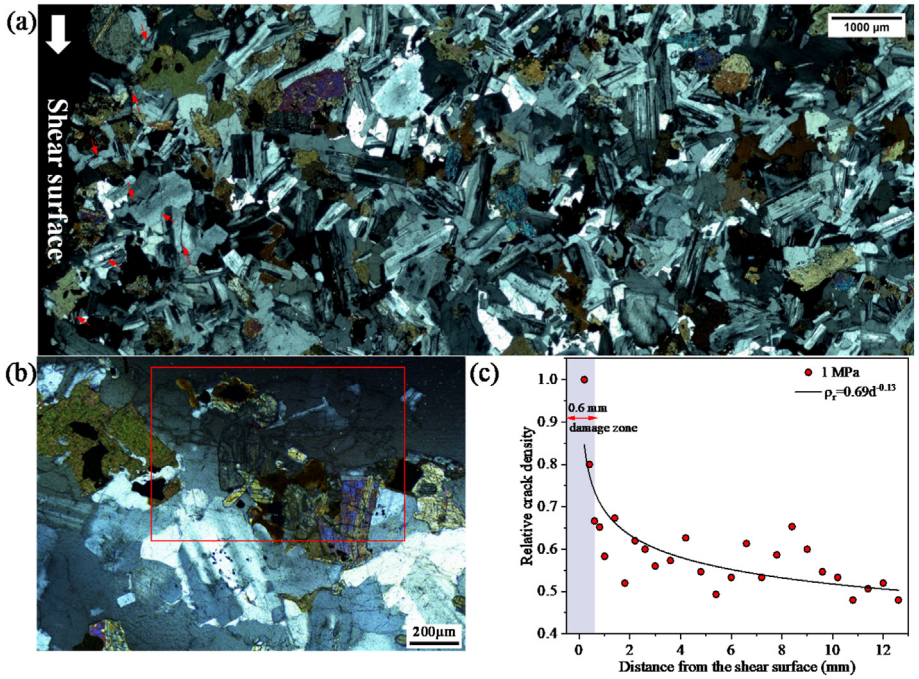

Fig. 15. (a) Micro-structure within the fault wall of rough joint under the normal stress of 1 MPa, (b) The shear surface with obvious cracks, and (c) Variation of relative crack density with increasing distance.

Please cite this article as: Meng F et al., Shear behavior and off-fault damage of saw-cut smooth and tension-induced rough joints in granite, Journal of Rock Mechanics and Geotechnical Engineering, https://doi.org/10.1016/j.jrmge.2023.07.008

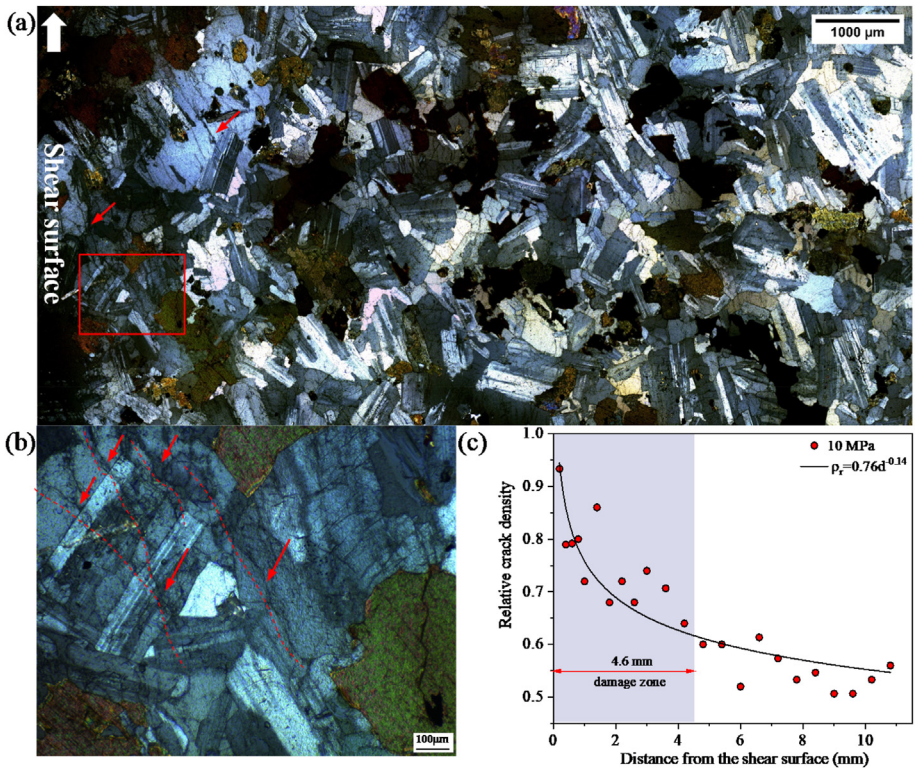

Fig. 16. (a) Micro-structure within the fault wall of rough joint under the normal stress of 10 MPa, (b) The zoom-in view of the area enclosed by the rectangle in (a), (c) Variation of relative crack density with increasing distance. The red arrows in (a) and (b) indicate the connected cracks, and the dashed lines in (b) show the propagation direction of the connected cracks.

shear. Based on the numerical study on two joints with different roughness sheared under the normal stress of 30 MPa in Meng et al. (2022), the largest contact force in the asperities is 220 MPa on the rougher surface (JRC of the profile is 14–16), while it is 140 MPa for the smoother surface (JRC of the profile is 6–8). Theses contact forces are nearly one order of magnitude larger than the applied normal stress. Besides, the micro-cracks are found to be more concentrated on the rougher joint surface which has a larger barrier for slip. Fewer cracks occur in the wall rock for the smoother joint but with more uniform distribution due to the smaller stress concentration.

4.2. Comparison with previous studies of the roughness effect on stick-slip

In earlier studies on the effect of surface roughness on the stick-slip failure of rock joints or faults (Okubo and Dieterich, 1984; Dieterich, 1978; Ohnaka and Shen, 1999; Tal et al., 2020), the surfaces of test rock blocks are generally polished to different surface roughness. These studies show that the greater the surface roughness, the lesser the tendency for stick-slip. For example, in the shear test of Okubo and Dieterich (1984) on two simulated fault surfaces with roughness of 0.2 μm and 80 μm, stress drops on the rough fault are found to be smaller than those on the smooth fault. Dieterich (1978) concluded that stick-slip occurs at lower normal stress for finely ground Westerly granite surfaces than it does for the rougher surface (the two surfaces had been respectively polished with abrasive of #600 and #240). Ohnaka and Shen (1999) found that the slip-weakening process during nucleation is less stable and more dynamic on a smoother fault, although the run-up distance and time are short on smooth fault surface than on rough, irregular fault surface. The conclusions of the above studies are different from the findings in the present study. Our direct shear tests show that there is no stick-slip (i.e. stable slip occurs) for the planar granite joint

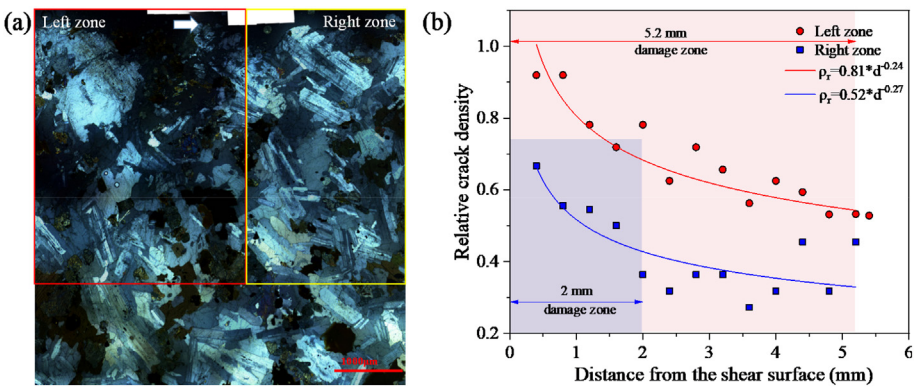

Fig. 17. (a) Micro-structure and (b) Variation of relative crack density with increasing distance of rough joint under 20 MPa normal stress.

Please cite this article as: Meng F et al., Shear behavior and off-fault damage of saw-cut smooth and tension-induced rough joints in granite, Journal of Rock Mechanics and Geotechnical Engineering, https://doi.org/10.1016/j.jrmge.2023.07.008

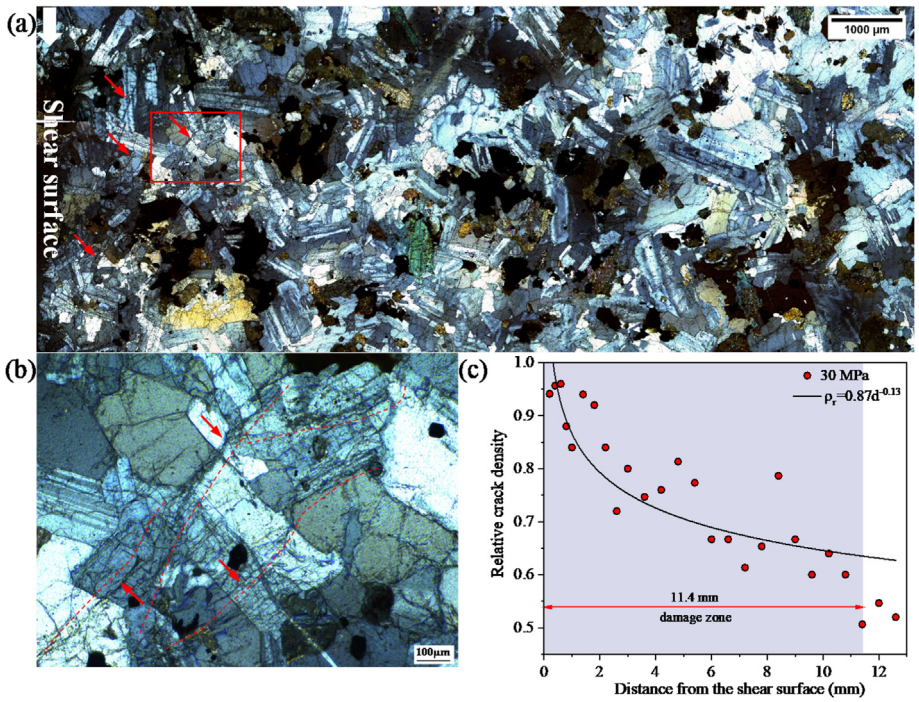

Fig. 18. (a) Micro-structure within the fault wall of rough joint under the normal stress of 30 MPa, (b) The zoom-in view of the area enclosed by the rectangle in (a), (c) Variation of relative crack density with increasing distance. The red arrows in (a) and (b) indicate the connected cracks, and the dashed lines in (b) show the propagation direction of the connected cracks.

surfaces sheared below the normal stress of 30 MPa. Only indistinctive stick-slip is observed during the second half of shear at the normal stress of 30 MPa, while unstable stick-slip takes place for the rough joints under all the normal stresses.

Morad et al. (2022) performed direct shear tests on laboratory faults with different surface conditions (tension fractures A and B, sawcut surface C, polished surfaces D and E, with RMS of 1356 μm, 450 μm, 7 μm, 0.85 μm and 0.7 μm respectively) under the same normal stress (5 MPa). Their study indicates that the stress drop is not monotonically correlated with the surface roughness. The stick-slip amplitude is the largest for the sawcut surface C which has a critical roughness, and it decreases with both the increase and decrease of surface roughness, in other words a much rougher or smoother surface will lead to stable slip of the fault. The critical roughness is the minimum roughness which is required for efficient mechanical interlocking of asperity contacts. For the polished surfaces with smaller roughness, the local stresses at the contacts of the asperities are too small to induce unstable sliding. In our study, the surfaces of the planar joints before shear are very smooth, and the mechanical interlocking and stress concentration of asperity contacts is inappreciable, which leads to the stable slip. Under a higher normal stress, the surface gradually becomes rougher with continuous slide (Fig. 6e and f), and the interlocking effect of asperity contacts becomes prominent, leading to large stress drops. Diabase and granite are respectively used in Morad et al. (2022) and the present study, and only 5 MPa normal stress is applied in the former study. The different rock types and the lower normal stress can account for the different frictional behavior for the roughest tension fractures. Stick-slip is more likely to occur in rocks with more quartz and sheared under a higher normal stress (Byerlee and Brace, 1968).

4.3. Stress-dependency of frictional behavior and damage of joints

The present study indicates that the level of normal stress plays a dominant role in determining the macro-shear behavior and micro-damage characteristics. For the saw-cut planar joints, the frictional sliding is stable even being sheared under the normal stress of 50 MPa until large stress drop occurs. The latter is associated with the large local fractures on the upper or bottom part of the joints, which is attributed to the sample preparation workmanship. Near the end of the shear tests, the regular stick-slip is also facilitated by the large normal stress, under which the gouges are adequately compacted to achieve high bonding strength.

For the rough joints which are obtained by open-mode tension, stick-slip occurs even under low normal stress (under the normal stress of 1 MPa, small amplitude stick-slip occurs). In terms of the normal stress of 5 MPa, the amplitude of stick-slip becomes more remarkable with increasing normal stress. The increase in stick-slip amplitude with increasing normal stress can be attributed to the increase in critical stiffness (Leeman et al., 2016; Tinti et al., 2016; Mei et al., 2021).

Our micro-observation shows that the thickness of the damage zone is larger under higher normal stress for both planar and rough joints, but it is different for the two groups of joints even under the same normal stress. A larger normal stress, which is associated with a higher local stress concentration in the asperities, leads to a larger extent of damage zone and more microcracks beneath the shear surface (Meng et al., 2022).

The gouges on the post-shear surface of planar joints increase with increasing normal stress (although the amount of gouge is generally much less than that of the rough joints) (Fig. 6), and more gouges are generated under normal stresses of 30 MPa and 50 MPa. Shear stress fluctuation occurs in the late stage of the shear test, rather than throughout the entire shear process under the normal stress of 30 MPa for the planar joint, which is closely related to the accumulation of gouge on the surface during shear. The amount of gouge increases with shear displacement, and the surface also becomes rougher (this inference is consistent with the slightly increasing trend of shear stress with shear displacement even towards the end of the test in Section 3.1 and Fig. 4). The gouge is

Please cite this article as: Meng F et al., Shear behavior and off-fault damage of saw-cut smooth and tension-induced rough joints in granite, Journal of Rock Mechanics and Geotechnical Engineering, https://doi.org/10.1016/j.jrmge.2023.07.008

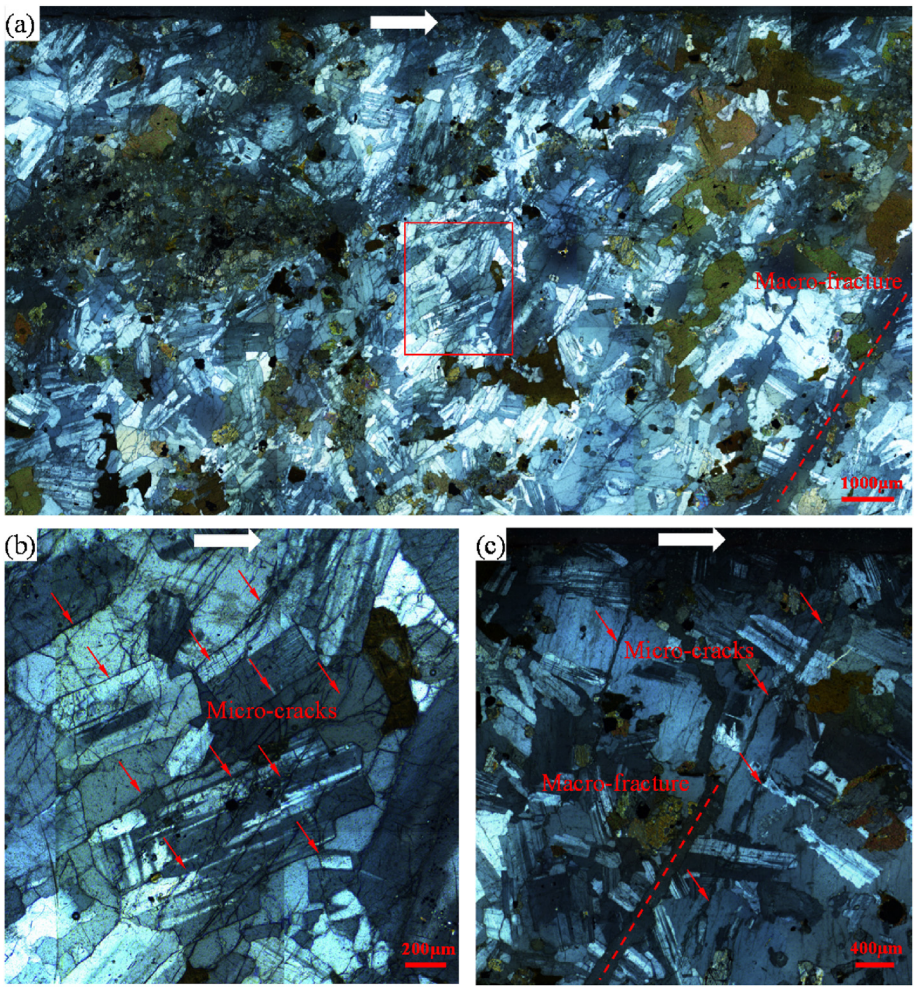

Fig. 19. (a) Off-fault damage of the planar joint under the normal stress of 50 MPa (50-2), (b) is the zoom-in view of the area enclosed by the rectangle in (a), and (c) is from the upper part of the joint adjacent to the shear surface.

compacted with continuous increase of slip under very high normal stress (Byerlee and Summers, 1976; Summers and Byerlee, 1977). Small stress drop takes place when local fractures occur in the compacted gouge particles.

Under the normal stress of 50 MPa, two shear stress-shear displacement curves differ with respect to the stress drops during shear (Fig. 5). The post-shear specimen of joint 50-2 is the most fractured among all the test planar and rough joints. A number of nearly parallel large tensile fractures occur in the upper part of the specimen (Fig. 6g), and several cracks are observed on the surface of the bottom part. In addition to these large macro-fractures, the constituent minerals between the fractures are severely cracked as observed on thin-sections (Fig. 19). The micro-cracks usually cut through multiple mineral grains. Moreover, these long micro-cracks are almost parallel with the macro-fractures (Fig. 19), and they are all inclined to the shear direction with acute angles. The comparison of Figs. 16, 18 and 19 suggests that both the coalesced micro-cracks and macro-fractures are inclined to the shear direction with acute angles under certain conditions whatever the roughness of the joints.

After shearing, since no large fractures occur on joint 50-1, and the mineral grains beneath the surface are also not severely cracked in comparison with those of joint 50-2, while the overall shear stress curves of the two joints are almost coincident, we consider that the large macro-fractures in joint 50-2 are closely related to the four large stress drops on the shear stress curves. When one large fracture is abruptly formed, the overall shear resistance of the joints drops simultaneously, leading to the large stress drop. The rock blocks are dissected by the fractures when subject to continuous shear, and the strength of the rock between fractures decreases due to the structure-weakening effect. Micro-cracks are easily formed under the joint effects of high normal stress and shear-tensile stress. The shear stress on the planar surface is more evenly distributed than that on the rough surface, which leads to different distribution patterns of the micro-cracks for the planar and rough joints in this study (the stress distribution is more complex on the rough surface, and the direction of the local stress acting on the contacting asperity is dependent on the shape of the asperities). The four large stress drops in joint 50–2 may be related to the sample preparation workmanship. Some small irregularities on the flat surface will lead to strong stress concentration under very high normal stress, resulting in large fractures and remarkable stress drops.

Regular stick-slip at the end of the test for joints 50-1 and 50-2 is attributed to the accumulation and compaction of gouges under higher normal stress, which is similar to the small stress oscillations under the normal stress of 30 MPa. These compacted gouges under higher normal stress fracture suddenly (Byerlee and Summers, 1976; Summers and Byerlee, 1977), or the force chain

Please cite this article as: Meng F et al., Shear behavior and off-fault damage of saw-cut smooth and tension-induced rough joints in granite, Journal of Rock Mechanics and Geotechnical Engineering, https://doi.org/10.1016/j.jrmge.2023.07.008

formed by the individual gouge particles ruptures abruptly, leading to the intermittent and remarkable stick-slip (Hayman et al., 2011).

4.4. Implications of the test results

Natural rock joint surfaces are characterized by different roughness. Our study shows that the planar joints become rougher with shear slip, and the smooth joints may fail unstably under high stress level because of the large local fractures and the accumulation of gouges. This indicates the possibility of unstable slip on planar joints (such as the fault slip rockburst, factitious earthquakes, etc) provided that the normal stress reaches a sufficiently high level. However, the off-fault damage beneath the shear surface, which is manifested by the detachment of mineral particles on the surface, is only restricted to a very thin top layer.

The generation and coalescence of the micro-cracks in the fault wall will create additional paths for flow of natural gas or liquid, thus increasing the permeability, which facilitates the recovery of subsurface resources such as gas, oil and enhanced geothermal energy. The very small thickness of the damage zone for the planar joints under normal stress ranging from 1 MPa to 50 MPa implies that the enhancement of permeability due to the initiation and connection of micro-cracks will be insignificant. In contrast, the much thicker damage zone and the larger numbers of micro-cracks in the fault wall of the tension-induced rough joints increase the rock permeability.

Moreover, those shear-induced micro-cracks will affect the pore pressure within the joints, fractures and faults. For the rough joints which have undergone certain amount of slip, the fault zone will not be completely sealed because of the presence of the connected cracks. As such, the liquid or gas escapes, which decreases the pore pressure within the faults and increases the effective normal stress acting on the fault. The fault is relatively sealed for the planar fault due to the lack of connected cracks in the fault wall, and the ejection of fluid into the fault will increase the pore pressure and thus decrease the effective normal stress, which will destabilize the faults.

5. Conclusions and future work

In this study, direct shear tests are conducted on saw-cut planar joints and tension-induced rough joints. The shear behavior and shear-induced micro-damage beneath the shear surface (i.e. the off-fault damage) for the planar and rough joints are quantified and compared. The key conclusions are:

(1) The saw-cut planar joints fail stably under almost all the applied normal stresses except under the normal stress of 50 MPa where regular stick-slip occurs close to the end the test, while both post-peak stress drop and stick-slip occurs for all the rough joints.
(2) The residual shear strength envelope of the rough joints and the peak shear strength envelope of the planar joints almost overlap, indicating that the residual friction angle of rough joints provides a good approximation of the basic friction angle.
(3) The RMS roughness increases after shear for the initially planar joints, while it decreases for the tension-induced rough joints.
(4) The shear-induced off-fault damage for the planar joints is restricted to a very thin layer, while a large number of micro-cracks develop in the minerals beneath the shear interface in addition to the shear-off of asperity tips for the rough joints.
(5) The thickness of the off-fault damage for rough joints is about an order of magnitude greater than that of the saw-cut planar joints under the same normal stress.

In this study, the macro-shear behavior and micro-off-fault damage characteristics of saw-cut planar and tension-induced rough joints under various normal stresses are examined. Our results indicate that resin coating on the post-shear surface effectively preserves the shear-induced damage for the joints. However, in this study, we only experiment this method to prepare thin-sections on selected planar joints due to the insufficient epoxy resin. In our future study, tests with a larger coverage for different joints are planned for a more comprehensive investigation on the shear-induced damage of different types of joint or fault.

The generation and coalescence of the micro-cracks in the fault wall will create additional paths for flow of natural gas or liquid, thus affecting the permeability and heat transfer efficiency. We only investigate the shear behavior of the two types of joints (i.e. saw-cut planar joints and tension-induced rough joints) and how the damage is influenced by normal stress in this study. Further study is warranted to quantify the permeability with the post-shear samples which contain the shear-induced cracks.

The mineral composition and grain size are known to affect the strength of granite. The shear behavior of rock joints is dependent on rock type and its micro-structures (Meng et al., 2017), and the ease of initiation and propagation of micro-cracks is closely related to the strength and bonding of different minerals. Therefore, the correlation between mineral type, grain size and the development and micro-structure of damage zone also deserves further research.

Declaration of competing interest

The authors declare that they have no known competing financial interests or personal relationships that could have appeared to influence the work reported in this paper.

Acknowledgments

We gratefully acknowledge financial support from Taishan Scholars Program (Grant No. 2019KJG002) and National Natural Science Foundation of China (Grant Nos. 42272329 and 52279116).

Appendix A. Supplementary data

Supplementary data to this article can be found online at https://doi.org/10.1016/j.jrmge.2023.07.008.

References

Alejano, L.R., Muralha, J., Ulusay, R., Li, C.C., Pérez-Rey, I., Karakul, H., Aydan, Ö., 2018. ISRM suggested method for determining the basic friction angle of planar rock surfaces by means of tilt tests. Rock Mech. Rock Eng. 51 (12), 3853–3859.
Alejano, L.R., Muralha, J., Ulusay, R., Li, C.C., Pérez-Rey, I., Karakul, H., Zhang, N., 2017. A benchmark experiment to assess factors affecting tilt test results for sawcut rock surfaces. Rock Mech. Rock Eng. 50 (9), 2547–2562.
Bandis, S.C., Lumsden, A.C., Barton, N.R., 1983. Fundamentals of rock joint deformation. Int. J. Rock Mech. Min. Sci. Geomech. Abstr. 20 (6), 249–268.
Barton, N.R., 1973. Review of a new shear-strength criterion for rock joints. Eng. Geol. 7 (4), 287–332.
Barton, N., Choubey, V., 1977. The shear strength of rock joints in theory and practice. Rock Mech. Rock Eng. 10, 1–54.
Barton, N., Quadros, D.E.F., 1997. Joint aperture and roughness in the prediction of flow and groutability of rock masses. Int. J. Rock Mech. Min. Sci. 34 (3–4).
Ben-Zion, Y., Sammis, C.G., 2003. Characterization of fault zones. Pure Appl. Geophys. 160 (3–4), 677–715.
Billi, A., Salvini, F., Storti, F., 2003. The damage zone-fault core transition in carbonate rocks: implications for fault growth, structure and permeability. J. Struct. Geol. 25 (11), 1779–1794.

Byerlee, J.D., Brace, W.F., 1968. Stick slip, stable sliding, and earthquakes-effect of rock type, pressure, strain rate, and stiffness. J. Geophys. Res. 73 (18), 6031–6037.
Byerlee, J., Summers, R., 1976. A note on the effect of fault gouge thickness on fault stability. Int. J. Rock Mech. Min. Sci. Geomech. Abstr. 13 (1), 35–36.
Chen, X., Madden, A.S.E., Reches, Z.E., 2017. Powder rolling as a mechanism of dynamic fault weakening. Fault zone dynamic processes: evolution of fault properties during seismic rupture. Geophysical Monograph 6, 133–150.
Dang, W.G., Tao, K., Chen, X., 2022. Frictional behavior of planar and rough granite fractures subjected to normal load oscillations of different amplitudes. J. Rock Mech. Geotech. Eng. 14 (3), 746–756.
Dang, W.G., Wu, W., Konietzky, H., Qian, J., 2019. Effect of shear-induced aperture evolution on fluid flow in rock fractures. Comput. Geotech. 114, 103152.
Dang, W.G., Konietzky, H., Frühwirt, T., Herbst, M., 2020. Cyclic frictional responses of planar joints under cyclic normal load conditions: laboratory tests and numerical simulations. Rock Mech. Rock Eng. 53 (1), 337–364.
Dieterich, J.H., 1978. Time-dependent Friction and the Mechanics of Stick-Slip. Rock Friction and Earthquake Prediction. Birkhäuser, Basel, pp. 790–806.
Goebel, T.H.W., Candela, T., Sammis, C.G., Becker, T.W., Dresen, G., Schorlemmer, D., 2014a. Seismic event distributions and off-fault damage during frictional sliding of saw-cut surfaces with pre-defined roughness. Geophys. J. Int. 196 (1), 612–625.
Goebel, T.H.W., Becker, T.W., Sammis, C.G., Dresen, G., Schorlemmer, D., 2014b. Off-fault damage and acoustic emission distributions during the evolution of structurally complex faults over series of stick-slip events. Geophys. J. Int. 197 (3), 1705–1718.
Guo, B., Fu, P., Hao, Y., Peters, C.A., Carrigan, C.R., 2016. Thermal drawdown-induced flow channeling in a single fracture in EGS. Geothermics 61, 46–62.
Hayman, N.W., Ducloué, L., Foco, K.L., Daniels, K.E., 2011. Granular controls on periodicity of stick-slip events: kinematics and force-chains in an experimental fault. Pure Appl. Geophys. 168 (12), 2239–2257.
Hencher, S.R., 2012. Discussion of Alejano, gonzalez and muralha (2012). Rock Mech. Rock Eng. 45, 1137–1139.
Hencher, S.R., Lee, S.G., Carter, T.G., Richards, L.R., 2011. Sheeting joints: characterisation, shear strength and engineering. Rock Mech. Rock Eng. 44 (1), 1–22.
Ji, Y., Hofmann, H., Duan, K., Zang, A., 2022a. Laboratory experiments on fault behavior towards better understanding of injection-induced seismicity in geoenergy systems. Earth Sci. Rev. 226, 103916.
Ji, Y., Wang, L., Hofmann, H., Kwiatek, G., Dresen, G., 2022b. High-rate fluid injection reduces the nucleation length of laboratory earthquakes on critically stressed faults in granite. Geophys. Res. Lett., e2022GL100418
Ji, Y., Wanniarachchi, W.A.M., Wu, W., 2020. Effect of fluid pressure heterogeneity on injection-induced fracture activation. Comput. Geotech. 123, 103–589.
Ji, Y., Wu, W., 2020. Injection-driven fracture instability in granite: mechanism and implications. Tectonophysics 791, 228572.
Jiang, Y., Li, B., Tanabashi, Y., 2006. Estimating the relation between surface roughness and mechanical properties of rock joints. Int. J. Rock Mech. Min. Sci. 43 (6), 837–846.
Lee, H.S., Cho, T.F., 2002. Hydraulic characteristics of rough fractures in linear flow under normal and shear load. Rock Mech. Rock Eng. 35, 299–318.
Leeman, J., Saffer, D., Scuderi, M.M., Marone, C., 2016. Laboratory observations of slow earthquakes and the spectrum of tectonic fault slip modes. Nat. Commun. 7, 11104.
Li, C., Zhang, N., Ruiz, J., 2019. Measurement of the basic friction angle of planar rock discontinuities with three rock cores. Bull. Eng. Geol. Environ. 78 (2), 847–856.
Lockner, D.A., Kilgore, B.D., Beeler, N.M., Moore, D.E., 2017. The transition from frictional sliding to shear melting in laboratory stick-slip experiments. Fault Zone Dynamic Process.: Evolut. Fault Propert. During Seismic Rupture 227, 105.
Mei, C., Barbot, S., Wu, W., 2021. Period-multiplying cycles at the transition between stick-slip and stable sliding and implications for the Parkfield period-doubling tremors. Geophys. Res. Lett. 48 (7), e2020GL091807.
Meng, F., Zhou, H., Wang, Z., Zhang, L., Kong, L., Li, S., Zhang, C., 2016. Experimental study on the prediction of rockburst hazards induced by dynamic structural plane shearing in deeply buried hard rock tunnels. Int. J. Rock Mech. Min. Sci. 86, 210–223.
Meng, F., Zhou, H., Wang, Z., Zhang, L., Kong, L., Li, S., Hu, S., 2017. Experimental study of factors affecting fault slip rockbursts in deeply buried hard rock tunnels. Bull. Eng. Geol. Environ. 76 (3), 1167–1182.
Meng, F., Zhou, H., Wang, Z., Zhang, C., Li, S., Zhang, L., Kong, L., 2018. Characteristics of asperity damage and its influence on the shear behavior of granite joints. Rock Mech. Rock Eng. 51 (2), 429–449.
Meng, F., Wong, L.N.Y., Zhou, H., Yu, J., Cheng, G., 2019. Shear rate effects on the post-peak shear behavior and acoustic emission characteristics of artificially split granite joints. Rock Mech. Rock Eng. 52 (7), 2155–2174.
Meng, F., Wong, L.N.Y., Zhou, H., Wang, Z., Zhang, L., 2020. Asperity degradation characteristics of soft rock-like fractures under shearing based on acoustic emission monitoring. Eng. Geol. 266, 105392.
Meng, F., Wong, L.N.Y., Guo, T., 2022a. Frictional behavior and micro-damage characteristics of rough granite fractures. Tectonophysics 842, 229589.
Meng, F., Song, J., Yue, Z., Zhou, H., Wang, X., Wang, Z., 2022b. Failure mechanisms and damage evolution of hard rock joints under high stress: insights from PFC2D modeling. Eng. Anal. Bound. Elem. 135, 394–411.
Mehrishal, S., Sharifzadeh, M., Shahriar, K., Song, J.J., 2016. An experimental study on normal stress and shear rate dependency of basic friction coefficient in dry and wet limestone joints. Rock Mech. Rock Eng. 49 (12), 4607–4629.
Mitchell, T.M., Faulkner, D.R., 2009. The nature and origin of off-fault damage surrounding strike-slip fault zones with a wide range of displacements: a field study from the Atacama fault system, northern Chile. J. Struct. Geol. 31 (8), 802–816.
Morad, D., Sagy, A., Hatzor, Y.H., 2020. The significance of displacement control mode in direct shear tests of rock joints. Int. J. Rock Mech. Min. Sci. 134, 104444.
Morad, D., Sagy, A., Tal, Y., Hatzor, Y.H., 2022. Fault roughness controls sliding instability. Earth Planet Sci. Lett. 579, 117365.
Moradian, Z.A., Ballivy, G., Rivard, P., Gravel, C., Rousseau, B., 2010. Evaluating damage during shear tests of rock joints using acoustic emission. Int. J. Rock Mech. Min. Sci. 47 (4), 590–598.
Moradian, Z.A., Ballivy, G., Rivard, P., 2012. Correlating acoustic emission sources with damaged zones during direct shear test of rock joints. Can. Geotech. J. 49 (6), 710–718.
Muralha, J., Grasselli, G., Tatone, B., Blümel, M., Chryssanthakis, P., Yujing, J., 2014. ISRM suggested method for laboratory determination of the shear strength of rock joints: revised version. Rock Mech. Rock Eng. 47 (1), 291–302.
Ohnaka, M., Shen, L.F., 1999. Scaling of the shear rupture process from nucleation to dynamic propagation: implications of geometric irregularity of the rupturing surfaces. J. Geophys. Res. Solid Earth 104 (B1), 817–844.
Okubo, P.G., Dieterich, J.H., 1984. Effects of physical fault properties on frictional instabilities produced on simulated faults. J. Geophys. Res. Solid Earth 89 (B7), 5817–5827.
Passelègue, F.X., Spagnuolo, E., Violay, M., Nielsen, S., Di Toro, G., Schubnel, A., 2016a. Frictional evolution, acoustic emissions activity, and off-fault damage in simulated faults sheared at seismic slip rates. J. Geophys. Res. Solid Earth 121 (10), 7490–7513.
Passelègue, F.X., Schubnel, A., Nielsen, S., Bhat, H.S., Deldicque, D., Madariaga, R., 2016b. Dynamic rupture processes inferred from laboratory microearthquakes. J. Geophys. Res. Solid Earth 121 (6), 4343–4365.
Patton, F.D., 1966. Multiple modes of shear failure in rock. In: Proceedings of the 1st Congress of International Society for Rock Mechanics, vol. 1, pp. 509–513. Lisbon, Portugal.
Power, W.L., Tullis, T.E., 1991. Euclidean and fractal models for the description of rock surface roughness. J. Geophys. Res. Solid Earth 96 (B1), 415–424.
Rowe, C.D., Lamothe, K., Rempe, M., Andrews, M., Mitchell, T.M., Di Toro, G., Aretusini, S., 2019. Earthquake lubrication and healing explained by amorphous nanosilica. Nat. Commun. 10 (1), 1–11.
Rohmer, J., Nguyen, T.K., Torabi, A., 2015. Off-fault shear failure potential enhanced by high-stiff/low-permeable damage zone during fluid injection in porous reservoirs. Geophys. J. Int. 202 (3), 1566–1580.
Sainoki, A., Mitri, H.S., 2014. Dynamic behavior of mining-induced fault slip. Int. J. Rock Mech. Min. Sci. 66, 19–29.
Summers, R., Byerlee, J., 1977. A note on the effect of fault gouge composition on the stability of frictional sliding. Int. J. Rock Mech. Min. Sci. Geomech. Abstr. 14 (3), 155–160.
Thomas, M.Y., Bhat, H.S., Klinger, Y., 2017. Effect of Brittle Off-Fault Damage on Earthquake Rupture Dynamics. Fault Zone Dynamic Processes: Evolution of Fault Properties during Seismic Rupture, pp. 227–255.
Tal, Y., Goebel, T., Avouac, J.P., 2020. Experimental and modeling study of the effect of fault roughness on dynamic frictional sliding. Earth Planet Sci. Lett. 536, 116133.
Tinti, E., Scuderi, M., Scognamiglio, L., Di Stefano, G., Marone, C., Collettini, C., 2016. On the evolution of elastic properties during laboratory stick-slip experiments spanning the transition from slow slip to dynamic rupture. J. Geophys. Res. Solid Earth 121 (12), 8569–8594.
Vogler, D., Amann, F., Bayer, P., Elsworth, D., 2016. Permeability evolution in natural fractures subject to cyclic loading and gouge formation. Rock Mech. Rock Eng. 49, 3463–3479.
Wang, C., Liu, R., Jiang, Y., Wang, G., Luan, H., 2022. Effect of shear-induced contact area and aperture variations on nonlinear flow behaviors in fractal rock fractures. J. Rock Mech. Geotech. Eng.
Wang, F., Wang, S., Yao, W., Li, X., Meng, F., Xia, K., 2023. Effect of roughness on the shear behavior of rock joints subjected to impact loading. J. Rock Mech. Geotech. Eng. 15 (2), 339–349.
Wang, F., Xia, K., Yao, W., Wang, S., Wang, C., Xiu, Z., 2021. Slip behavior of rough rock discontinuity under high velocity impact: experiments and models. Int. J. Rock Mech. Min. Sci. 144, 104831.
Xiu, Z., Meng, F., Wang, F., Wang, S., Ji, Y., Hou, Q., 2023. Shear behavior and damage evolution of the interface between rough rock and cemented tailings backfill. Theor. Appl. Fract. Mech. 125, 103887.
Yamashita, F., Fukuyama, E., Xu, S., Mizoguchi, K., Kawakata, H., Takizawa, S., 2018. Rupture preparation process controlled by surface roughness on meter-scale laboratory fault. Tectonophysics 733, 193–208.
Yang, B., Jiang, Q., Feng, X., Xin, J., Xu, D., 2022. Shear testing on rock tunnel models under constant normal stress conditions. J. Rock Mech. Geotech. Eng. 14 (6), 1722–1736.
Zhang, L., Cong, Y., Meng, F., et al., 2021. Energy evolution analysis and failure criteria for rock under different stress paths. Acta Geotech 16 (2), 569–580.

Please cite this article as: Meng F et al., Shear behavior and off-fault damage of saw-cut smooth and tension-induced rough joints in granite, Journal of Rock Mechanics and Geotechnical Engineering, https://doi.org/10.1016/j.jrmge.2023.07.008

Zhang, L., Chao, W., Liu, Z., et al., 2022. Crack propagation characteristics during progressive failure of circular tunnels and the early warning thereof based on multi-sensor data fusion. Geomech. Geophys. Geo-energ. Geo-resour. 8, 172.

Zhou, J.Q., Hu, S.H., Fang, S., Chen, Y.F., Zhou, C.B., 2015. Nonlinear flow behavior at low Reynolds numbers through rough-walled fractures subjected to normal compressive loading. Int. J. Rock Mech. Min. Sci. 80, 202–218.

Zhao, Q., Tisato, N., Kovaleva, O., Grasselli, G., 2018. Direct observation of faulting by means of rotary shear tests under X–ray micro–computed tomography. J. Geophys. Res. Solid Earth 123 (9), 7389–7403.

Zhao, Z., Li, B., Jiang, Y., 2014. Effects of fracture surface roughness on macroscopic fluid flow and solute transport in fracture networks. Rock Mech. Rock Eng. 47 (6), 2279–2286.

Zhou, X., Shou, Y., Yang, L., He, Y., 2020. Stick-slip failure in heterogeneous sheared fault with a variety of fault roughness. Phys. Earth Planet. In. 309, 106587.

Zielke, O., Galis, M., Mai, P.M., 2017. Fault roughness and strength heterogeneity control earthquake size and stress drop. Geophys. Res. Lett. 44 (2), 777–783.

Dr. Fanzhen Meng received his PhD degree at the Institute of Rock and Soil Mechanics, Chinese Academy of Sciences in 2015, and worked as a post-doctoral research fellow (Hong Kong Scholar) in Department of Earth Sciences, The University of Hong Kong from 2018 to 2020. He is now a professor in Qingdao University of Technology (QUT). His research interests include (1) brittle rock fracturing mechanism and evaluation in the lab and field; (2) Rockburst and induced seismicity in deep tunneling/mining and subsurface energy recovery and (3) Shear failure and reactivation of rock fractures, joints and faults and the related geohazard. He has coauthored more than 60 peer-review research papers, and one of the papers was selected as “Most cited articles published in JRMGE since 2021". He won the Excellent Doctoral Dissertation Award of Chinese Academy of Science and Outstanding Doctoral Dissertation Award of the CSRME.

Please cite this article as: Meng F et al., Shear behavior and off-fault damage of saw-cut smooth and tension-induced rough joints in granite, Journal of Rock Mechanics and Geotechnical Engineering, https://doi.org/10.1016/j.jrmge.2023.07.008